lubricants

MDPI

Article

The Influence of Pulsed Electron Beam Processing on the Quality of Working Surfaces of Titanium Alloy Products

Undrakh Mishigdorzhiyn [1,2,*], Aleksey Pyatykh [3], Andrey Savilov [3], Nikolay Ulakhanov [2,4], Ivan Galetsky [2], Kirill Demin [2], Alexander Tikhonov [3], Maxim Vorobyov [5], Elizaveta Petrikova [5] and Shunqi Mei [1,*]

1 Hubei Digital Textile Equipment Key Laboratory, Wuhan Textile University, Wuhan 430073, China
2 Institute of Physical Materials Science, Siberian Branch of the Russian Academy of Sciences, 670047 Ulan-Ude, Russia; nulahanov@mail.ru (N.U.); ivan.galetskiy@bk.ru (I.G.); kirill.demin.19992@gmail.com (K.D.)
3 School of Aircraft Construction, Mechanical Engineering and Transport, Irkutsk National Research Technical University, 664074 Irkutsk, Russia; pyatykhas@ex.istu.edu (A.P.); saw@istu.edu (A.S.); tihonovalex90@mail.ru (A.T.)
4 Department of Mechanical Engineering, East Siberia State University of Technology and Management, 670013 Ulan-Ude, Russia
5 Institute of High Current Electronics, Siberian Branch of the Russian Academy of Sciences, 634055 Tomsk, Russia; vorobyovms@yandex.ru (M.V.); elizmarkova@yahoo.com (E.P.)
* Correspondence: mishigdorzh@gmail.com (U.M.); sqmei@wtu.edu.cn (S.M.)

Abstract: Titanium alloys are widely used in medicine due to their unique properties, including inertness with respect to living tissues, light weight, high strength, and impact toughness. For successful implementation, titanium alloy implants should possess high wear resistance and hydrophilicity. This article investigates the surface modification process of VT-1 and VT-6 titanium alloys by electron-beam processing (EBP). The EBP effect on the modified surface's wear resistance, roughness, and hydrophilicity was analyzed. The specimens were made by machining them at a CNC turning center. The specimen surfaces were modified at the SOLO facility by a submillisecond modulated electron beam with a controlled power density of thermal impact, allowing it to reach and stabilize 1400 °C in 400 μs and then maintain it on the surface for 600 μs. A friction machine with a counterbody was used to study the wear resistance of the specimen surface. The study revealed that EBP reduces the roughness parameters of the surface. EBP also decreases the contact angle of wetting, indicating an increase in hydrophilicity compared to the original surface. Experimentally, it was shown that the formation of a nanostructure consisting of needle-like α-strips induced by EBP improves the wear resistance of the surface layer.

Keywords: titanium alloy; implants; electron source; plasma cathode; pulsed electron beam processing; wear resistance; Ti-Ti friction pair; hydrophilicity; roughness; biomedicine

check for updates

Received: 7 March 2025
Revised: 11 April 2025
Accepted: 25 April 2025
Published: 28 April 2025

Citation: Mishigdorzhiyn, U.; Pyatykh, A.; Savilov, A.; Ulakhanov, N.; Galetsky, I.; Demin, K.; Tikhonov, A.; Vorobyov, M.; Petrikova, E.; Mei, S. The Influence of Pulsed Electron Beam Processing on the Quality of Working Surfaces of Titanium Alloy Products. *Lubricants* **2025**, *13*, 199. https://doi.org/10.3390/lubricants13050199

Copyright: © 2025 by the authors. Licensee MDPI, Basel, Switzerland. This article is an open access article distributed under the terms and conditions of the Creative Commons Attribution (CC BY) license (https://creativecommons.org/licenses/by/4.0/).

1. Introduction

Titanium alloys are widely used in the aviation industry, special mechanical engineering, engine building, and biomedical industry due to their low density, high specific strength, heat resistance, corrosion resistance in the biological environment, and bio- and mechanical compatibility with living tissues. Consequently, osteosynthesis products made from Grade 5 Ti-6Al-4V alloy (an analog of VT-6) are currently considered more promising than products made from stainless steel and cobalt alloys. This is because the latter contains a large amount of nickel and chromium, which can form disordered solid solutions in the base metal and readily release toxic ions into the body [1–5]. The Grade 1 unalloyed Ti

alloy (an analog of VT-1) is also used in producing implants, but it is not as widespread as VT-6 due to its worse mechanical properties [6].

Both alloys are known to have low wear resistance, which limits their application in areas involving wear and friction [7]. Alam et al. [8] revealed significant delamination of the Ti-6Al-4V specimen material during dry sliding against hardened steel counterbodies. Similarly, Kang et al. [9] concluded that the low wear resistance of Ti-6Al-4V is linked to forming a fragile, loosened oxide layer.

The tribological properties of titanium alloys (wear resistance, friction coefficient, and hardness) can be improved through surface modification methods such as thermal oxidation, PVD, electrochemical anodization (EA), thermal–chemical treatment (TCT), laser alloying, and electron beam processing (EBP) [3,10,11].

Thermal oxidation improves the chemical resistance, adhesion, mechanical strength, and durability of titanium surfaces [12,13]. Thermal oxidation entails heating the titanium surface to a lower temperature in oxygen or another oxidizing gas, which contributes to forming an oxide layer on the titanium surface. This oxide layer improves the titanium surface properties and makes titanium more resistant to harmful substances. Titanium surface treatment by thermal oxidation is an effective way to improve the properties of the titanium surface, allowing for its expanded application in various industries, including radio space, aerospace, and automotive industries. PVD coatings are also used to improve the biocompatibility of implants, such as artificial joints or stents, preventing corrosion, improving tissue growth, or increasing the rate of tissue regeneration. Due to their wear resistance, antibacterial properties, and ability to control coating thickness, PVD coatings are one of the most popular methods to improve medical devices and instruments. However, this method has certain limitations: the thin coating layer, typically a maximum of 5 μm, may be inadequate for some applications. Furthermore, the process requires specialized equipment and highly skilled personnel, which complicates the use of the technology and increases costs.

Among the EA and TCT methods used for modifying titanium surfaces in medical implants are anodization, nitriding, carburization, and functionalized coating [14]. Anodization involves immersing titanium in an electrolytic solution and applying an electrical current to form an oxide coating on the surface. This coating can improve cell adhesion to the implant, improving integration with the surrounding tissue. Nitriding introduces nitrogen into the surface layer of titanium, thereby improving the material′s hardness, wear resistance, and biocompatibility. Furthermore, it can improve cell growth and bone tissue regeneration. Carburization forms a carbide layer on the titanium surface, improving its hardness and wear resistance. This can improve the durability of implants. Functionalized coatings entail heat-treating titanium to form surfaces with enhanced hydrophilicity, increased antibacterial activity, or drug retention capacity. These processes improve titanium′s surface properties, making it better suited for medical implants, such as orthopedic prostheses, dental implants, and other medical devices. However, the aforementioned treatment methods possess drawbacks. For example, anodization is difficult to manage in terms of coating thickness, surface roughness, and porosity. Furthermore, residual aluminum oxide particles following treatment can be risky in the post-implantation phase due to aluminum's potential toxicity. Nitriding presents difficulties in regulating pore size and surface roughness. In addition, there is a risk of developing undesirable consequences in the post-implantation phase due to the effect of nitrogen on the body. These disadvantages are inherent in carburization and functionalized coating.

Laser alloying improves the properties by adding additional elements or alloys [15]. This process enhances titanium implants′ biocompatibility, mechanical strength, and wear resistance. Laser alloying involves several steps. First, the titanium implant surface is

cleaned of contaminants and oxides. Then, a layer of the alloying material, such as nitinol or a titanium-zirconium alloy, is applied. Finally, the surface is irradiated with a laser, which increases the temperature and causes the melting of the upper layer of the titanium, fusing it with the applied material. After completion of the process and solidification of the material, the surface becomes stronger and more resistant to wear and corrosion. This method allows for precise control of the penetration depth of the added material and its uniform distribution over the surface, which ensures high accuracy and increased efficiency of the modification process. Laser alloying of titanium surfaces is an effective method for improving the properties of implants, making them more durable and biocompatible. The disadvantage of this method is the high cost of equipment, which reduces its availability. Laser alloying has limitations, including material suitability, structural changes, and part geometry restrictions. The high processing temperature can cause structural alterations, leading to deformations and defects. Moreover, laser alloying is constrained by the size and shape of parts, presenting challenges when dealing with large products.

EBP is an effective way of modifying the titanium surface to improve implant biocompatibility and biological activity [16]. This method changes the physical and chemical properties of the titanium surface, making it more suitable for interaction with body tissues. EBP begins with cleaning the titanium surface of contaminants and oxides. Then, the surface is irradiated with a high-energy electron flow, which causes microroughness and changes in the surface layer composition. This process improves cell adhesion to the implant surface and stimulates bone tissue growth. The modified layer can improve the biological activity of titanium and its mechanical properties, such as hardness and wear resistance. In addition, surface modification can reduce the risk of corrosion and allergic reactions to the implant material. Therefore, EBP can be utilized in the production of modern implants, providing better biocompatibility and material durability. During the EBP, an electron beam generated by an electron accelerator is directed onto the material surface. The electrons interact with atoms and molecules upon impact, causing structural changes on the surface or internal structure. EBP can be used for various purposes, such as enhancing the strength and hardness of materials, changing their electrical properties, modifying surfaces, and creating thin films. The advantages of EBP include the process's accuracy and controllability, the ability to process a wide range of materials (metals, polymers, ceramics, etc.), and the capacity to create complex geometric structures.

Various technological methods have been studied to improve the functional properties of osteosynthesis products made of titanium alloys [6–8]. The long-term stability of implants is mainly influenced by osteointegration, which begins with the contact between the implant surface and bone tissue. After this contact, bone tissue cells move to the implant surface and adhere to it, creating osteoblasts responsible for synthesizing the bone matrix. Osteoblasts precipitate mineral salts, forming new bone tissue around the implant. After osseointegration, the implant becomes inextricably linked with the bone tissue, ensuring strong fixation. Many studies have focused on modifying titanium implant surfaces and their roughness [17,18].

Additive manufacturing (AM) is also gaining popularity in modern medical practice [19]. AM is applied in the production of medical devices, such as dental implants, orthopedic implants, or bone templates. AM involves creating objects by adding material layer by layer based on a digital model. Its advantages for producing implants are individualization (the ability to create unique implants for specific needs), accuracy (accurate reproduction of the implant design according to a digital model), efficiency (accelerating the production process and reducing the waiting time), and improved strength (implants are stronger and more durable). Although AM is highly productive and can be

used for creating complex shapes, finishing is required due to the high roughness of the working surfaces [20].

EBP is a promising technology for finishing biomedical products. Its efficiency has repeatedly been demonstrated, including using an electron source with a plasma cathode developed by the Institute of High-Current Electronics SB RAS (Tomsk) [21–24]. For instance, Koval et al. reported on the surface polishing of a transosseous osteosynthesis device using pulsed EBP [24].

Thus, EBP was determined as an effective and promising surface engineering technique after analyzing titanium surface modification methods. The current research aims to establish the effect of pulsed EBP, as a finishing operation after 3-D printing and mechanical processing, on the wear resistance, roughness, and hydrophilicity of the working surfaces of titanium alloy products used in biomedicine.

2. Materials and Methods

Titanium is a difficult-to-machine material, comparable to cast iron and stainless steel. Machining titanium alloys is significantly more labor-intensive than machining ordinary steel, requiring 2 to 2.5 times more effort. Furthermore, during titanium processing, the contact area between the tool's cutting edge and the chips is smaller than in steel machining. Due to the low thermal conductivity of titanium, the tool heats up strongly, especially in the contact zone with the chips. When processing steel, the temperature in the cutting zone reaches 300–350 °C; when cutting titanium alloys, it reaches 1100–1200 °C. With an increase in cutting speed, the temperature in the contact area increases. Therefore, relatively low cutting speeds from 5 to 80 m/min are used for titanium machining [25].

Titanium alloy specimens, made from VT-1 and VT-6 alloy bars in forged condition after annealing (analogs of Grade 1 and Grade 5 alloys according to the ASTM standard, respectively), were used for the research. The chemical compositions of titanium alloys are presented in Tables 1 and 2. The machining was performed on a NEF 400 DMG MORI Co., Ltd., Tokyo, Japan CNC turning center using an SDJCL 2020K 11, Sandvik Coromant, Sandviken, Sweden turning cutter equipped with H13A carbide inserts. Previously, the machining of titanium alloys and the factors affecting their operational properties were investigated [26,27]. The results of these studies are used in the aviation and biomedical industries. The geometric parameters of the cutting tool were as follows: side cutting edge angle $\psi = 93°$, rake angle $\gamma = 0°$, inclination angle of the main cutting edge $\lambda = 0°$, relief angle $\alpha = 7°$. The cutting speed was Vc = 70 m/min, feed–fn = 0.2 mm/rev, and cutting depth–ap = 3 mm. The specimens were cut in the shape of cylinders with a diameter of 10 mm and a height of 8 mm (Figure 1).

Table 1. Chemical composition of VT-1 alloy, wt%.

Fe	C	Si	N	Ti	O	H	Impurities
up to 0.25	up to 0.07	up to 0.1	up to 0.04	99.24–99.7	up to 0.2	up to 0.01	0.3

Table 2. Chemical composition of VT-6 alloy, wt%.

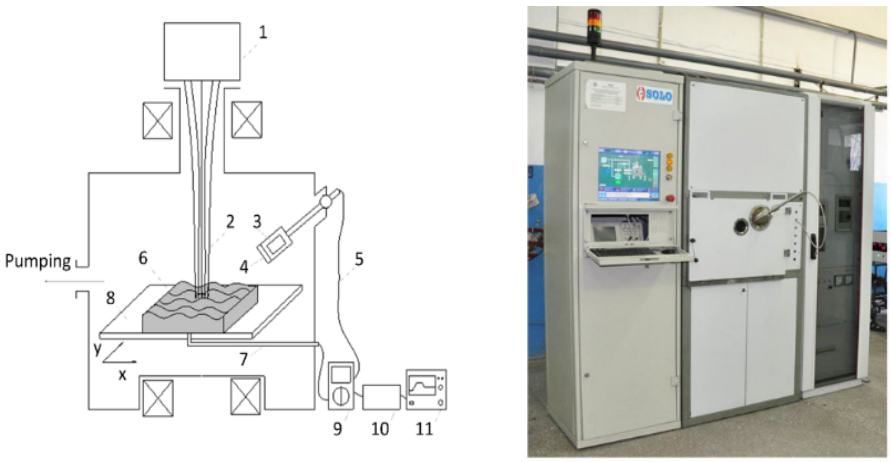
Fe	C	Si	V	N	Ti	Al	Zr	O	H	Impurities
up to 0.6	up to 0.1	up to 0.1	3.5–5.3	up to 0.05	86.45–90.9	5.3–6.8	up to 0.3	up to 0.2	up to 0.015	0.3



Figure 1. The specimens after machining before EBP.

After machining, the specimens were subjected to EBP at the IHCE SB RAS (Tomsk, Russia), where various electron sources and accelerators with plasma cathodes have been developed and created over the decades [28,29]. The SOLO electron source is one with a plasma cathode based on a low-pressure arc discharge. It has no global analogs regarding the combination of its parameters [30]. Today, the SOLO electron source allows the generation of electron beams with diameters of up to 7 cm, energy of up to 25 keV, and energy density of up to 100 J/cm^2 at a pulse duration of 20–2000 s [31–36]. The possibility of controlling the beam current, which is weakly dependent on the accelerating voltage, is the unique feature of this type of electron source. Thus, it is possible to control the beam power in the sub-millisecond range of pulse durations [33,34] and, hence, the rate of energy input to the surface of a treated target within a beam current pulse [35]. The control of input energy makes it possible to control the temperature field in the target surface layer and, hence, its structure and phase state.

Just as in [37,38], irradiation with a modulated electron beam occurred in a vacuum chamber at an argon pressure of 35 mPa under a guiding magnetic field up to 100 mT. Figure 2 shows a schematic diagram of electron-beam irradiation. The specimens *6* were fixed on a two-coordinate manipulator *8* with a narrow stainless steel plate with a thickness of 0.2 mm and a height of 5–7 mm for thermal-loss reduction. The specimens were moved in the vacuum chamber under electron beam *2* using the manipulator table. The temperature of the specimen surface was measured with a high-speed infrared pyrometer *10* (KGA 740-LO, KLEIBER Infrared GmbH, Unterwellenborn, Germany), allowing temperature measurements in the range of 300–2300 °C with a response time of 6 µs. The pyrometer used radiation at 2–2.2 µm, which was collected by lens *11* with a surface-spot diameter of about 5 mm at the specimen center. The output signal of the pyrometer was the voltage measuring 0–10 V, which depended linearly on the temperature in the operating range of 2000 °C.



(**a**) (**b**)

Figure 2. Processing scheme (**a**) and appearance (**b**) of the SOLO facility: 1—plasma electron source; 2—electron beam; 3—objective; 4—quartz glass; 5—fiber optic cable; 6—specimen; 7—thermocouple; 8—manipulator table; 9—multimeter; 10—high-speed infrared pyrometer; 11—oscilloscope.

The electron energy during the treatment did not exceed 15 keV, which minimizes the requirements for the radiation safety of personnel. The radial distribution of the thermal energy density delivered to the specimen was a Gaussian curve with a width of about 3 cm. The surface was treated with three pulses, each separated by a 3 s interval. The plasma cathode discharge current, which directly controls the beam current, was altered during a pulse of ≈1000 μs within 20–65 A, resulting in a temperature of ~1400 °C on the specimen surface 400 μs after the beginning of the exposure and was maintained for the next 600 μs, as indicated in the oscillogram in Figure 3. The electron beam processing mode was selected in such a way as to ensure controlled heating of the specimen surface to a temperature above the melting point and subsequent quenching from the melt at a cooling rate of up to 10^7 K/s [39]. The defective substructure of the VT6 titanium surface layer changes and a nanostructure is formed as a result of this treatment, which increases its mechanical characteristics [40].

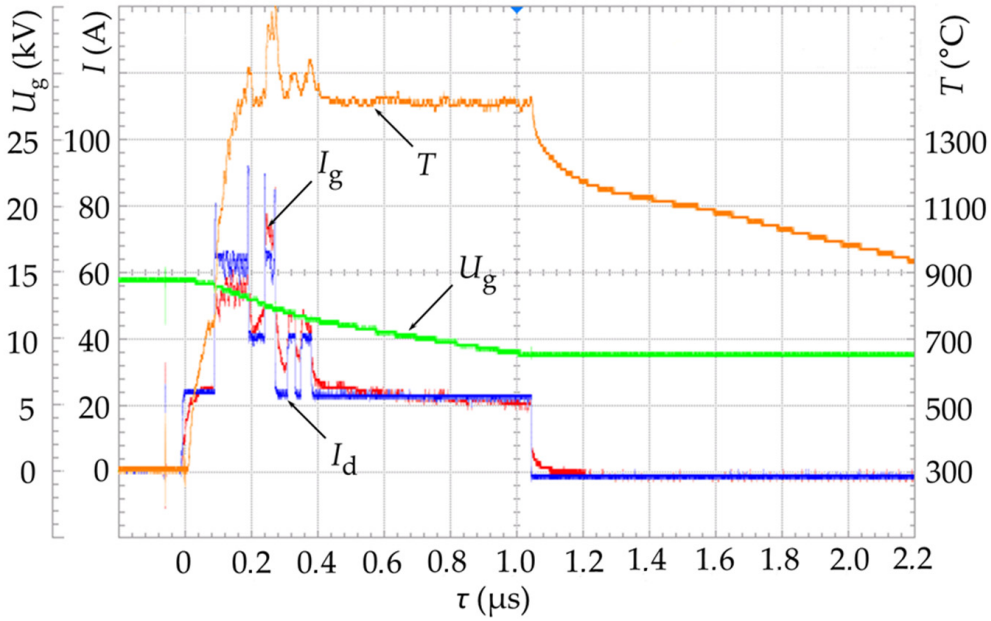
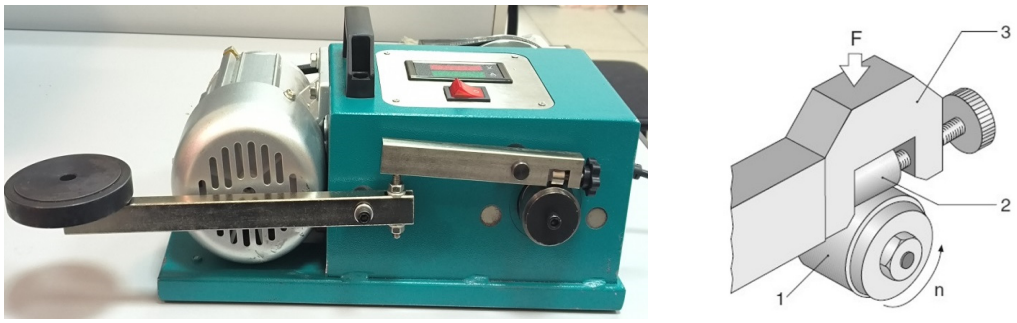


Figure 3. Oscillograms of the plasma cathode discharge current: I_d—of the plasma cathode discharge current; I_g—current in the accelerating gap; U_g—accelerating voltage [kV]; T—high-speed pyrometer output signal [°C].

The microstructure of the specimens was studied with an Altami MET 2C, Altami LLC, Saint Petersburg, Russia metallographic microscope and a JSM-6510LV, JEOL Ltd, Tokyo, Japan scanning electron microscope (SEM) with an acceleration voltage of 20 keV at the Science Center "Progress" of the East Siberia State University of Technology and Management, Ulan-Ude, Russia (ESSUTM). A microhardness tester PMT-3M (JSC LOMO, St. Petersburg, Russia) was used. A pyramid indented with an angle of 136° between opposite faces at a load of 100 gf was applied with 10 s for each download, hold, and upload at a constant strain rate. The average value of 5 prints was taken to avoid dismissal. XRD analysis was conducted on a D2 PHASER, Bruker AXS GmbH, Karlsruhe, Germany diffractometer with a LYNXEYE linear detector, in copper radiation with a shooting interval of 10–90°. The measurement step was 0.020, and the processing time for one step was 1.2 s.

Subsequently, the specimens underwent testing on a friction machine (Figure 4a) to evaluate their resistance to surface wear under EBP conditions. Wear resistance was assessed using a "crossed cylinders" configuration (Figure 4b). A rotating counterbody made from VT-6 titanium alloy with an outer diameter of 40 mm, a width of 11 mm, and a hardness of 30 ± 2 HRC was used (Figure 5). This counterbody was manufactured on

a DMG NEF 400 turning center and finished to a surface roughness of Ra 1.8 μm. The hardness of the test specimens was 15 ± 1 HRC for the VT-1 alloy and 30 ± 2 HRC for the VT-6 alloy, respectively.



(**a**) (**b**)

Figure 4. The friction machine (**a**) and the diagram of wear resistance studies (**b**), where 1 is a counterbody, 2 is a specimen, and 3 is a lever with a specimen lock.



Figure 5. The counterbody is made from VT-6 alloy.

The specimens were tested for three minutes; the pressing force to the counterbody was F = 150 N, and the linear sliding speed was 1 m/s. Each specimen underwent three wear resistance tests. The mass of each specimen before and after the experiment was determined on an A&D HR-150AZ, Tokyo, Japan analytical balance with a resolution of 0.0001 g.

A method measuring the contact angle and quantitatively assessing the adhesive properties (hydrophilicity) of titanium alloy specimens before and after exposure to EBP was employed. The method enables the quantitative evaluation of metal surface wettability and correlation with surface adhesion properties. The results can be applied to optimize EBP parameters to enhance the hydrophilicity/hydrophobicity of the titanium alloy surfaces. The test was conducted using the sessile drop method at an ambient temperature of 25 °C and relative humidity of 30–60%, utilizing a laboratory setup (Figure 6).

According to the hydrophilicity test, a 20 μL droplet of distilled water was deposited onto the fixed sample placed on the three-axis adjustable stage using the variable-volume pipette. The contact angle was measured using an optical microscope. The measurement result was the average of 5 parallel measurements. Subsequently, the droplet's angle θ was determined through image projection analysis using ToupView software (Windows Microscope ToupView Package 2025.01.15. (Figure 7).

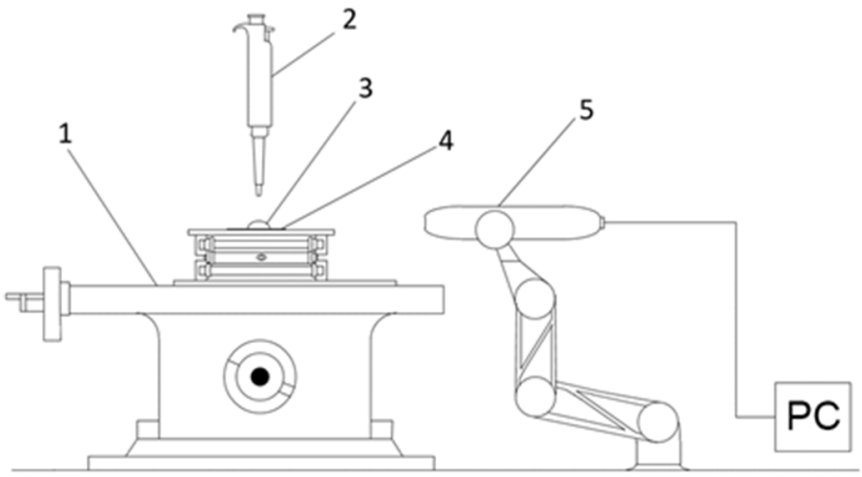


Figure 6. The scheme of the contact angle measurement setup, where 1 is the 3-axis positioning stage, 2 is the adjustable-volume laboratory pipette, 3 is a distilled water droplet, 4 is the test specimen, and 5 is an optical microscope.

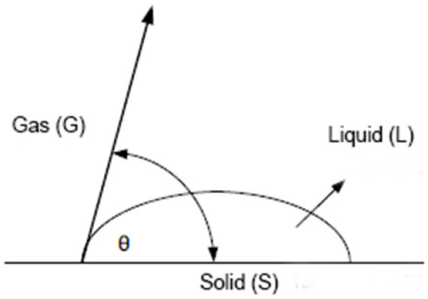


Figure 7. Schematic representation of the contact angle θ formed between the tangent line and the specimen surface.

3. Results

Processing on the SOLO facility using the previously mentioned modes results in a high-speed (≈$6.5 \cdot 10^6$ K/s) heating on the target surface by an electron beam with controllably variable with a high power density (up to 120 kW/cm^2 according to estimates taking into account previously published data [31] and calorimetric measurements of the energy density per pulse), causing high-speed melting and recrystallization. Figure 8 shows the impact scheme. It was established that the microhardness of the VT-1 alloy increased by 2.5 times, from approximately 131–163 HV to 400–450 HV, after EBP at electron energy 20 J/cm^2, pulse duration 100–150 μs, and 3 pulses with a 0.3 s interval.

The most crucial roughness parameter in implantology is the average roughness depth (*Sa*) [41]. For implantology, *Sa* is assessed to determine the quality of the implant surface. This indicator evaluates the degree of roughness of the implant surface and its ability to integrate with the surrounding bone tissue. The average roughness depth *Sa* affects the adhesion of cells to the bone, ensuring a stronger and more stable attachment of the implant. The higher this indicator, the better the adhesion of the implant to the bone tissue, which contributes to successful osteointegration and increases the implant′s durability.

Thus, measuring *Sa* in implantology allows for selecting the appropriate implant with optimal surface characteristics for specific cases, improving the prediction of successful and long-lasting results. The working surfaces of implants can be classified as follows according to this roughness parameter: (1) smooth surfaces ($Sa < 0.5$ μm); (2) slightly rough surfaces ($Sa = 0.5$–1 μm); (3) moderately rough surfaces ($Sa = 1$–2 μm); and (4) rough surfaces ($Sa > 2$ μm).

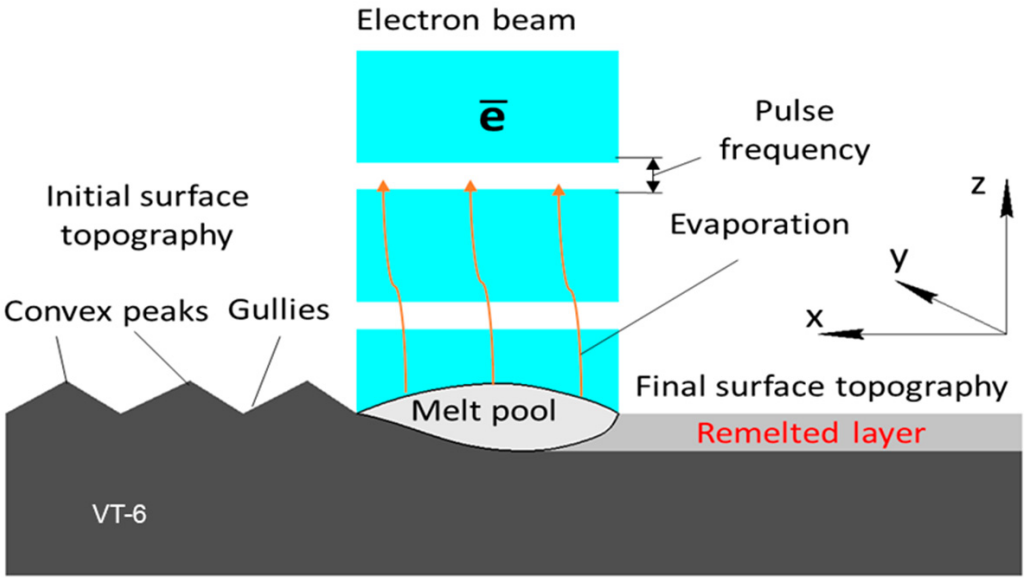


Figure 8. Scheme of pulsed electron beam polishing.

It was established that the EBP of titanium alloy rolled products contributes to a more favorable result in terms of surface quality. Figure 9 shows the three-dimensional topographies of specimen surfaces. EBP following turning improves the surface quality of the specimens; the profile becomes more regular, and peaks and irregularities are smoothed out. The *Sa* of the rolled specimen exposed to turning and subsequent EBP decreases almost twofold from 0.373 μm to 0.193 μm.

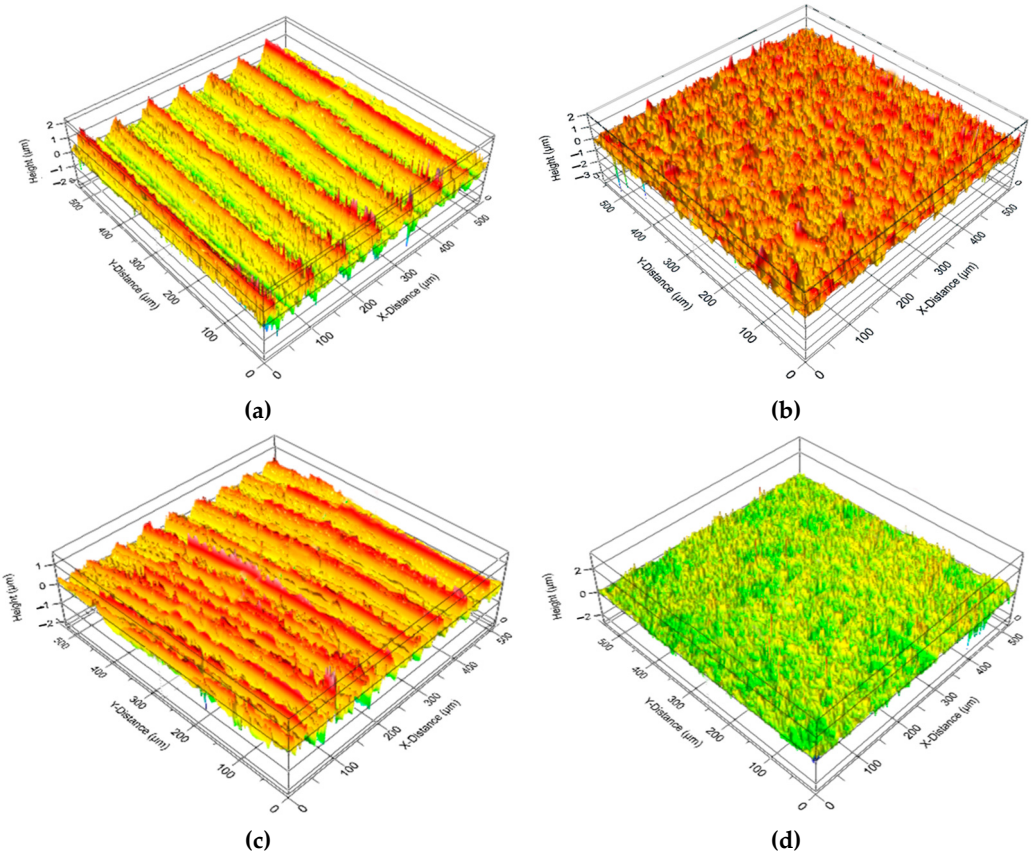


Figure 9. Three-dimensional surface topographies of specimens: (**a**) VT-1 after turning; (**b**) VT-1 after EBP; (**c**) VT-6 after turning; (**d**) VT-6 after EBP.

EBP is accompanied by melting and microroughness evaporation and the movement of the melt under the action of surface tension forces filling the pores. Macro images are provided to assess the surface quality in Figure 10. These macrophotographs and images of the specimen surface obtained using SEM after turning (Figure 10a,c) and after EBP (Figure 10b,d) revealed no traces of mechanical processing on the specimen subjected to EBP. The surface was smooth and uniform on the macrophotograph, and the SEM image revealed a granular microstructure with a grain dimension of about 10 μm.

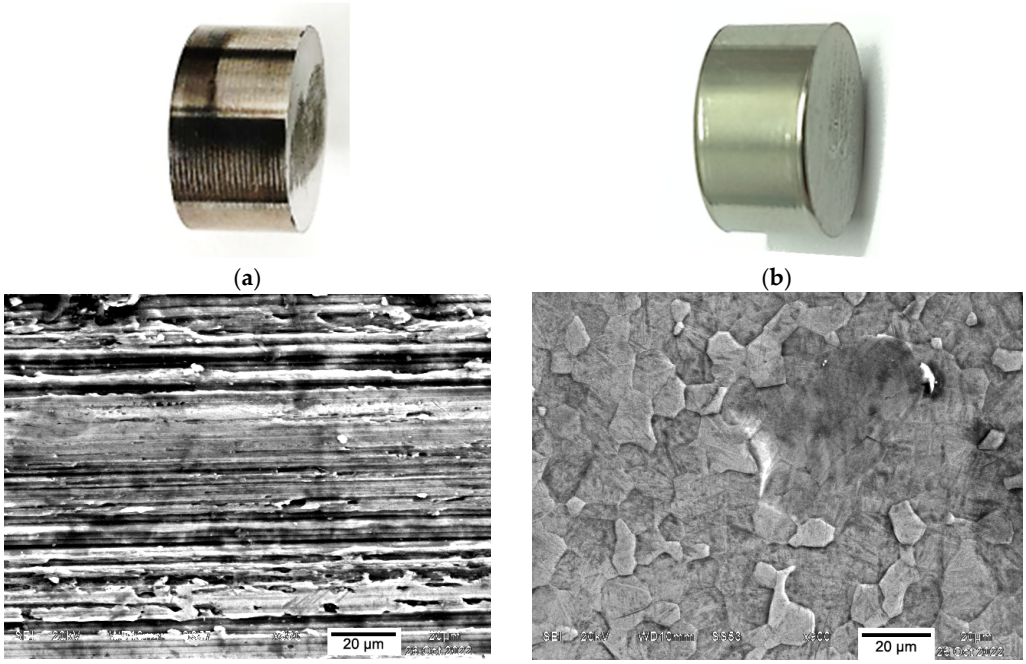


Figure 10. Macro and SEM images of the surface of specimens (**a**,**c**) before and (**b**,**d**) after EBP.

The metallographic analysis revealed that the base metal of the as-rolled alloys exhibits large α-phase grains separated by layers of the β-phase (Figure 11a). After EBP, the surface layer had a refined nanostructure with small α-phase grains (Figure 11b). The resulting microstructure shows extreme refinement, consisting of needle-like α-laths with an average width of approximately 0.49 μm and 10–20 μm length. Furthermore, numerous ultrafine secondary precipitates were observed at the α-lath interfaces. The electron beam′s thermal effect extended to 30–35 μm depth. Magnified SEM pictures revealed β-phase precipitations in the base metal and α-laths in the modified zone (Figure 11c,d). The XRD analysis revealed no change in phase composition (Figure 12). However, the intensity of the peaks is drastically reduced, and their bases are broadened, which is attributed to the grain refinement process. In addition, diffraction angles for crystalline planes were slightly shifted to the right from their original position due to the residual stress induced by EBP.

The tribological properties of titanium alloys are crucial in applying these materials in all industries, but they are essential in medicine. Titanium and some of its alloys are known for their relatively high friction coefficient and low tribological characteristics. However, electron beam treatment reduces the friction coefficient and decreases the wear rate, making it more attractive for use in friction and sliding conditions. Previous research by the coauthors revealed a decrease in the friction coefficient by 1.4 times that of the VT-1 alloy after EBP [42]. The low friction coefficient reduces energy losses and ensures more efficient system operation and corrosion resistance.

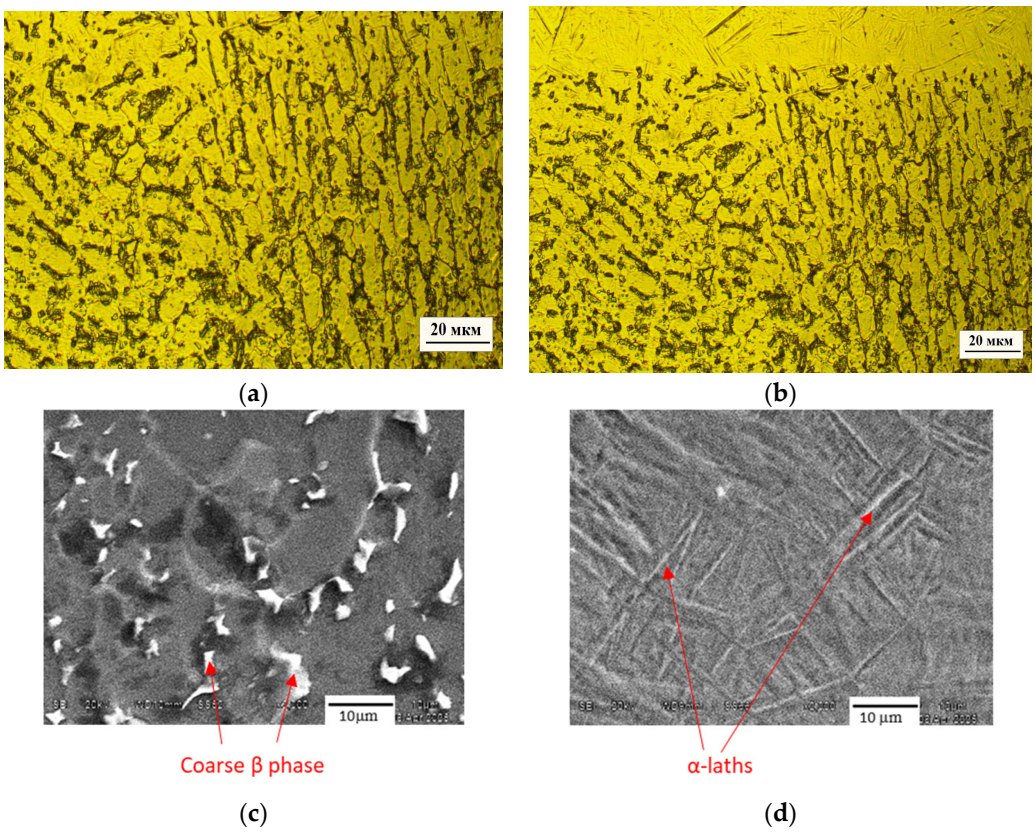


Figure 11. The microstructure of the VT-6 alloy specimen: optical microscopy (**a**) before and (**b**) after EBP; SEM (**c**) base metal and (**d**) modified zone.

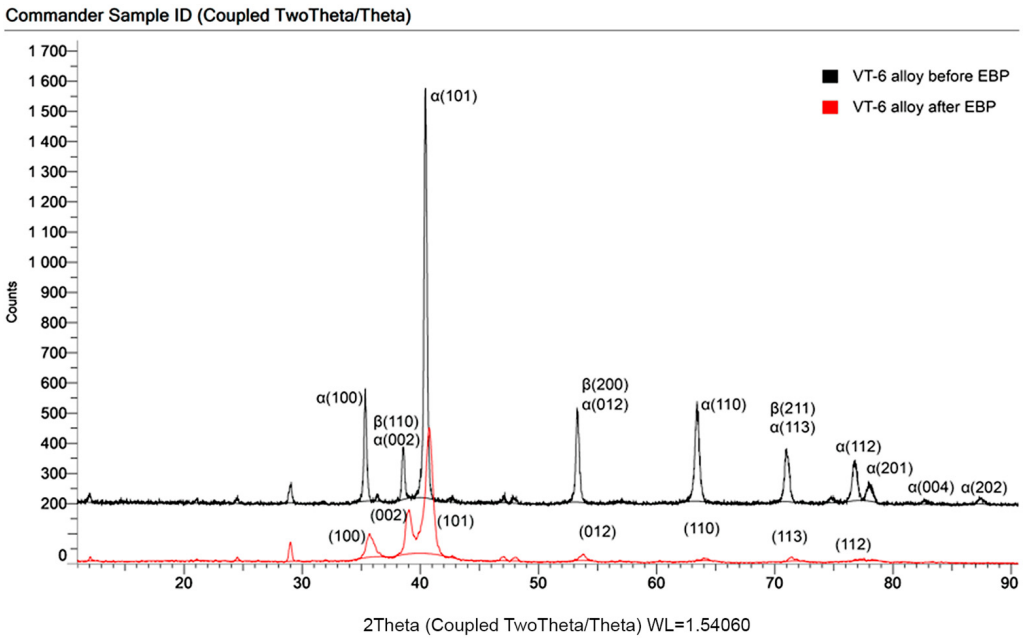
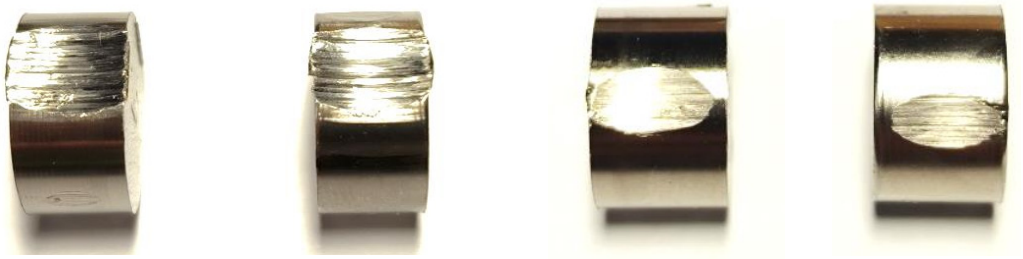


Figure 12. XRD patterns of specimens from VT-6 alloy before and after EBP.

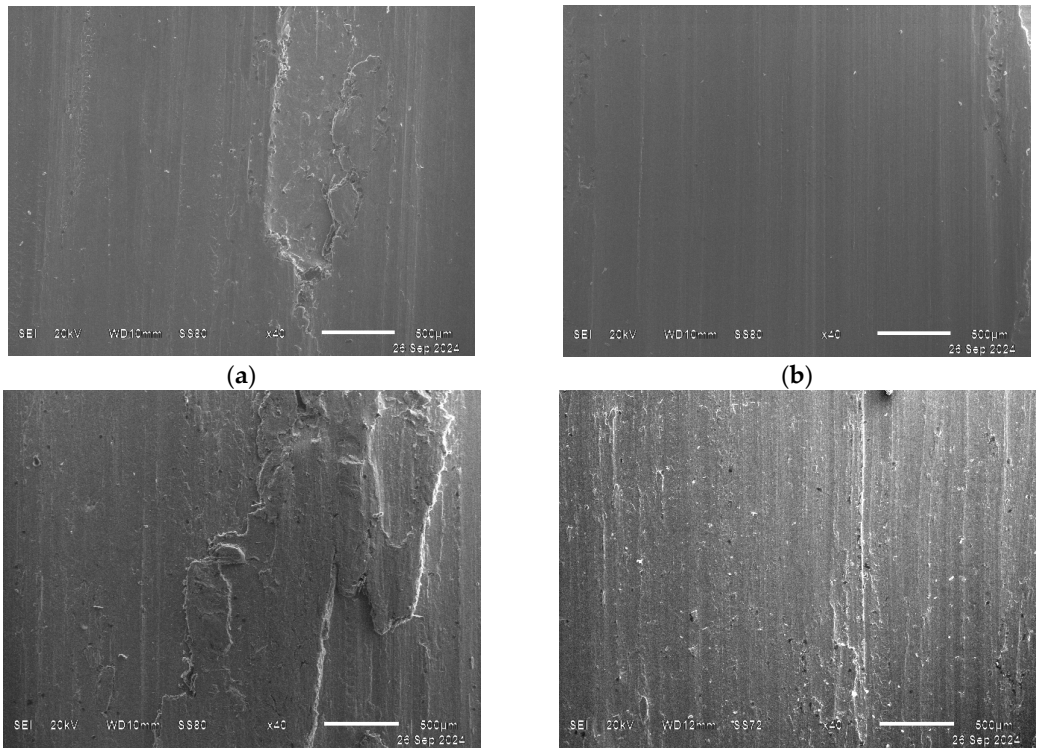
The tribological properties of titanium alloys may vary depending on their composition, processing, operating conditions, and interaction with other materials. It is essential, therefore, to carry out additional studies to determine the tribological properties of specific titanium alloys under peculiar operating conditions. Figure 13 shows macrographs of VT-1 and VT-6 alloy specimens after wear resistance testing. Due to the twofold difference in the

hardness of the alloys (131–163 MPa for VT-1 and 255–341 MPa for VT-6, according to HB 10^{-1}), the difference in wear can be observed. The fractographic analysis of the specimens after wear resistance testing revealed differences in the wear mechanism before and after EBP (Figure 14). For example, large peeling areas are observed on the wear surfaces of titanium alloys before EBP (Figure 14a,c), indicating predominantly adhesive wear. The wear surface on the VT-1 alloy after EBP repeats the relief of the counterbody, leaving vertical grooves on the modified surface (Figure 14d). Preferential abrasive wear is also observed on the surface of the VT-6 alloy after EBP (Figure 14b). In this alloy, impurities act as abrasives, manifesting as dark and light dispersed particles on the wear surface. Evidence of adhesive wear is also present, characterized by localized areas of material tearing.



(**a**) (**b**) (**c**) (**d**)

Figure 13. Titanium alloy specimens after wear resistance testing: (**a**) VT-1 before EBP; (**b**) VT-1 after EBP; (**c**) VT-6 before EBP; (**d**) VT-6 after EBP.



(**a**) (**b**) (**c**) (**d**)

Figure 14. SEM images of wear surfaces on titanium alloys: (**a**) VT- before EBP; (**b**) VT-1 after EBP; (**c**) VT-6 before EBP; (**d**) VT-6 after EBP.

Wear resistance tests demonstrated a lower mass loss rate for specimens after EBP than for untreated specimens (Figure 15). For example, mass loss (Δm) for the VT-1 alloy decreased by 0.0129 g and the VT-6 by 0.0056 g after EBP under the specified load and test duration. The formation of a refined nanostructure, consisting of needle-like α-laths,

following EBP, enhances the surface layer's wear resistance. A previous study [42] reported increased microhardness and wear resistance and decreased friction coefficient for the VT-1 alloy after EBP, attributable to surface layer modification. This structural refinement, extending to a depth of up to 50 μm, is achieved during high-speed cycling with five repeating electron beam pulses, facilitating multiple α↔β phase transformations.

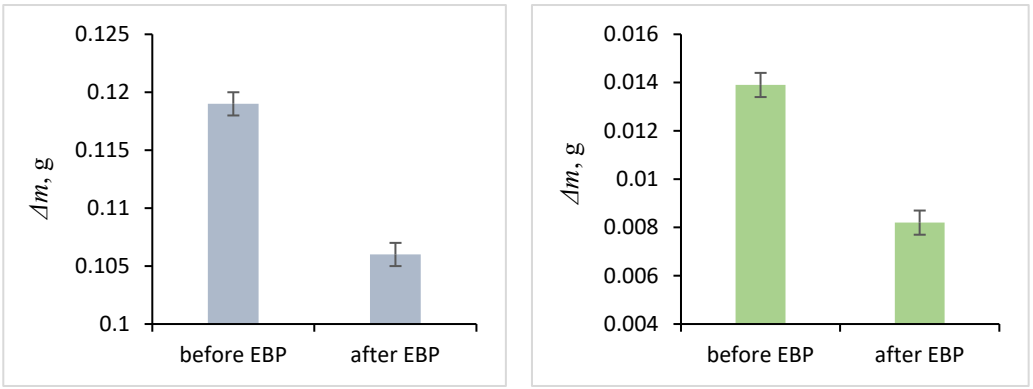


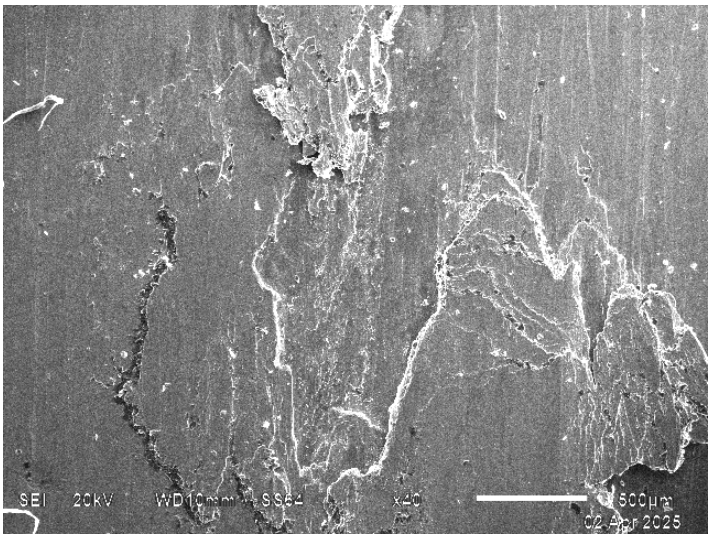
Figure 15. Wear resistance of specimens before and after EBP: (**a**) VT-1 alloy; (**b**) VT-6 alloy.

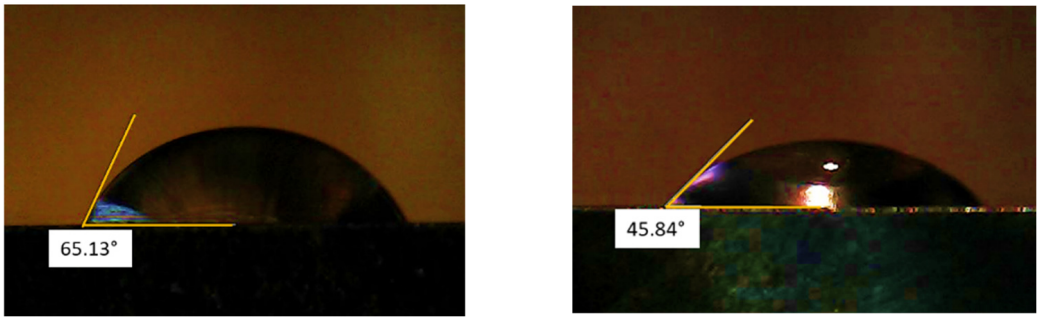
Rapid wear of an untreated surface may be associated with the loosening of the oxide layer. A loose oxide layer on the surface of titanium alloys reduces the mechanical and operational properties of the material and may also complicate various technological operations. This type of oxide layer can be formed during thermal oxidation of a damaged surface with voids and microcracks. A complex surface treatment is used to remove such layers, including loosening in alkaline solutions or melts and subsequent acid etching. Sometimes, pre-machining is required, such as sandblasting or hydroblasting.

An EDS analysis of the worn surface of the counterbody showed oxidation occurred during the interaction with the test specimen of VT-6 before EBP (Table 3). Delaminated craters and smeared adhesion lumps characterize the damaged surface. Such a surface was formed due to intense adhesive material transfer and its following plastic deformation, resulting in the galling build-up. It is known that Ti-Ti tribo pairs possess a tendency to gall when coming into contact with each other. Delamination is the primary wear mechanism attributed to adhesive wear, the same as VT-6 before EBP.

Titanium materials used in biomedicine must provide a set of properties, including hydrophilicity, which contributes to the faster integration of the material with the tissues of a living organism. The contact angle of a water drop on a flat surface determines the hydrophilicity or wettability of a surface. It was reported that the non-treated Ti-6Al-4V alloy contact angle is in the range of 64 to 92.8° [43,44]. Figure 16 shows the contact angles of wetting for the specimens made from VT-6 alloy after mechanical treatment and EBP. The measurement shows that the EBP decreases the contact angle of wetting from ~65° to ~46°, which indicates an increase in the hydrophilicity compared to the original surface. Thus, EBP can be a finishing polishing process to reduce roughness and create special properties of working surfaces. The contact angle reduction increases cell attachment and facilitates titanium implant integration into the body.

Table 3. SEM image of wear surfaces on the ring counterbody of VT-6 alloy and its chemical composition.

	Elemental Composition, wt%			
	O	Al	Ti	V
	8.43	5.41	82.38	3.79



(**a**) (**b**)

Figure 16. The results of determining the contact angles of wetting with water for specimens from VT-6: (**a**) after machining; (**b**) after EBP.

4. Discussion

Experiments showed that EBP results in surface roughness reduction and wear resistance enhancement. The latter is associated with microstructure transformation, e.g., grain refinement and quenching induced by high cooling rate. Toh et al. [45] reported on alternate microstructures mixed with acicular α′ martensite in Ti-6Al-4V (Ti64) parts obtained additive manufactured by the powder-bed-based electron beam melting (EBM) technique. In addition, the authors explained the XRD peak shifting phenomenon by the presence of martensite. Similar types of microstructures were obtained after the laser welding of Ti-6Al-4V alloy joints [46]. It has been reported that cooling rates higher than 410 °C/s should be achieved to obtain a fully martensitic microstructure in the Ti6Al4V alloy.

The reduction in the roughness parameter *Sa* positively affects the wear resistance of the contact surfaces of implants, such as hip joint endoprostheses. At the same time, a low value of the *Sa* parameter may impair the mechanical fixation of the bone implant and negatively impact osteointegration without a bioactive coating, taking into account the low attachment capability of human stromal cells to smooth titanium surfaces. There is no literature on the optimal surface roughness of Ti implants. Some sources indicate moderately rough, hydrophilic surfaces influence osteoprogenitor cell adhesion, proliferation, and differentiation in osteoblasts [47].

In our opinion, rough surfaces are necessary for the conjunction with the living tissue (bones) for osteointegration, while smooth surfaces are for the contract area with other implant parts (e.g., collar in dental implants) or moving body parts interacting as a friction pair. Summarized roughness parameters are given in Table 4. It is shown that EBP technology ensures surface quality equal to polishing [48].

Table 4. Comparative surface roughness *Sa* [48–50].

Treatment	Surface Roughness (*Sa*), μm
Polished implant collar	0–0.4
Smooth machining	0.5–0.9
Ti plasma spray	5.2
Double acid etching	0.5–0.9
Sandblasting, acid etching	1.6–2.6
Anodization	1.7–2
EBP (Current research)	0.193

The Ti-Ti friction pairs are rare compared to Ti-other materials friction pairs. However, some biomedical applications involve the same material combination, such as Ti screws or plates [51]. The Ti-Ti friction pairs have some features, like a high coefficient of friction (0.4–0.6) and a tendency to adhesive wear. The formation of abrasive particles can cause inflammation in a living organism. Protective coatings (PVD, DLC) can prevent this process. In the past few years, various films and coatings, including high-entropy alloys (HEAs), have gained recognition by demonstrating attractive and unique properties compared with conventional film materials. Several techniques have been developed for the production of films and coatings, including magnetron sputtering [52–54], laser cladding [55,56], spraying [57], electrodeposition [58], plasma transfer arc cladding [59], and other methods. Compared with bulk material sintering technologies, such as arc melting technology or casting methods, synthesizing HEA films and coatings can more easily achieve a rapid cooling rate, the so-called "quick quenching" effect, due to their smaller thickness. This is very important in forming coatings and films of high-energy alloys since high-energy alloys can undergo various phase transformations during slow cooling due to the decrease in the thermodynamic driving force at lower temperatures. Moreover, a high cooling rate can limit the diffusion of elements and inhibit the nucleation and growth of intermetallic compounds, which is essential in creating high-quality coatings for medical purposes [59,60].

Further study of the current research may be associated with continuing tribological testing to assess the friction coefficient and residual stress distribution within the modified zone and oxidation resistance testing. Other EBP modes for surface modification can be tested, and new approaches, such as electron beam surface alloying, seem promising for further expansion of the scope of titanium alloys.

5. Conclusions

The EBP process is accompanied by the melting and evaporation of the heights of microroughness and the movement of the melt under the action of surface tension forces, filling the pores. Consequently, the surface quality, as measured by the *Sa* parameter, improves twofold (from 0.373 μm to 0.193 μm). EBP also enhances surface hydrophilicity, indicated by a reduced contact angle. Furthermore, the EBP induces the grain refinement and formation of acicular α' martensite to a depth of 35 μm from the surface. The obtained structure enhances the mechanical properties of Ti alloys, such as microhardness and wear resistance. Wear resistance tests revealed a lower mass loss rate for the specimens after EBP than before EBP. Specifically, EBP reduced mass loss by 10% for VT-1 specimens and 40% for VT-6 specimens.

Author Contributions: Conceptualization, A.P., A.S. and U.M.; methodology, N.U., K.D., A.T. and I.G.; validation, K.D. and E.P.; investigation, A.P., N.U. and A.T.; resources, I.G.; data curation, E.P.; writing—original draft preparation, A.P., A.S. and S.M.; writing—review and editing, A.S., U.M. and S.M.; supervision, A.S. and M.V.; project administration, M.V.; funding acquisition, S.M. All authors have read and agreed to the published version of the manuscript.

Funding: The work was supported by the Russian Science Foundation (project no. 20-79-10015-P).

Data Availability Statement: Data are contained within the article.

Acknowledgments: The authors are grateful to Pavel Moskvin, a researcher at the Institute of High Current Electronics of the Siberian Branch of the Russian Academy of Science; and Ivan Polyansky, a researcher at the East Siberia State University of Technology and Management for assistance in experiments and analyses.

Conflicts of Interest: The authors declare no conflicts of interest.

References

1. Kollerov, M.; Spektor, V.; Skvortsova, S.; Mamonov, A.M.; Gusev, D.E.; Gurtovaya, G.V. Problems and prospects for use of titanium alloys in medicine. *J. Titan.* **2015**, *48*, 42–53.
2. Jagadesh, T.; Samuel, G.L. Investigation into cutting forces and surface roughness in micro turning of titanium alloy using coated carbide tool. *Procedia Mater. Sci.* **2014**, *5*, 2450–2457. [CrossRef]
3. Geetha, M.; Singh, A.K.; Asokamani, R.; Gogia, A.K. Ti based biomaterials, the ultimate choice for orthopaedic implants—A review. *Prog. Mater. Sci.* **2009**, *54*, 397–425. [CrossRef]
4. Abbas, A.T.; Sharma, N.; Anwar, S.; Luqman, M.; Tomaz, I.; Hegab, H. Multi-response optimization in high-speed machining of Ti-6Al-4V using TOPSIS-fuzzy integrated approach. *Materials* **2020**, *13*, 1104. [CrossRef]
5. Pramanik, A.; Guy, L. Machining of Titanium Alloy (Ti-6Al-4V)-Theory to Application. *Mach. Sci. Technol.* **2015**, *19*, 1–49. [CrossRef]
6. Nikolaeva, E.; Chapyshev, A.; Spitsyn, A. Technological Characteristics of Production of Implants from Titanium and Alloys Based. *Key Eng. Mater.* **2022**, *910*, 314–320. [CrossRef]
7. Budinski, K.G. Tribological properties of titanium alloys. *Wear* **1991**, *151*, 203–217. [CrossRef]
8. Alam, M.O.; Haseeb, A.S.M.A. Response of Ti–6Al–4V and Ti–24Al–11Nb alloys to dry sliding wear against hardened steel. *Tribol. Int.* **2002**, *35*, 357–362. [CrossRef]
9. Kang, K.-T.; Koh, Y.-G.; Son, J.; Yeom, J.S.; Park, J.-H.; Kim, H.-J. Biomechanical evaluation of pedicle screw fixation system in spinal adjacent levels using polyetheretherketone, carbon-fiberreinforced polyetheretherketone, and traditional titanium as rod materials. *Compos. B Eng.* **2017**, *130*, 248–256. [CrossRef]
10. Johnson, R.; Eberhardt, J. *Thermal Oxidation: A Promising Surface Treatment for Titanium Engine Parts*; Transportation Program, Oak Ridge National Laboratory: Oak Ridge, TN, USA, 2006.
11. Liu, X.; Chu, P.K.; Ding, C. Surface modification of titanium, titanium alloys, and related materials for biomedical applications. *Mater. Sci. Eng. R Rep.* **2004**, *47*, 49–121. [CrossRef]
12. Güleryüz, H.; Çimenoğlu, H. Effect of thermal oxidation on corrosion and corrosion–wear behaviour of a Ti–6Al–4V alloy. *Biomaterials* **2004**, *25*, 3325–3333. [CrossRef] [PubMed]
13. Li, Y.; Zhao, C. Advanced interconnect technology and reliability. In *Woodhead Publishing Series in Electronic and Optical Materials, CMOS Past, Present and Future*; Radamson, H.H., Luo, J., Simoen, E., Zhao, C., Eds.; Woodhead Publishing: Cambridge, UK, 2018; pp. 215–247. [CrossRef]
14. Revankar, G.D.; Shetty, R.; Rao, S.S.; Gaitonde, V.N. Wear resistance enhancement of titanium alloy (Ti–6Al–4V) by ball burnishing process. *J. Mater. Res. Technol.* **2017**, *6*, 13–32. [CrossRef]
15. Chengwei, C.; Zhiming, Z.; Xitang, T.; Wang, Y.; Sun, X.T. Influence of rapidly solidified structures on wear behavior of Ti-6AI-4V laser alloyed with TiC. *Tribol. Trans.* **1995**, *38*, 875–878. [CrossRef]
16. Soskova, N.; Vashchuk, E.S.; Budovskih, E.A.; Gromov, V.E.; Rajkov, S.V.; Ivanov, Y.F.; Losinskaya, A.A.; Pavlyukova, D.V. Electron-beam treatment of titanium VT1-0 surface after electroexplosive carburizing with zirconium oxide. *Met. Work. Mater. Sci.* **2013**, *58*, 37–41.
17. Shi, L.-Y.; Wang, A.; Zang, F.-Z.; Wang, J.-X.; Pan, X.-W.; Chen, H.-J. Tantalum-coated pedicle screws enhance implant integration. *Colloids Surf. B* **2017**, *160*, 22–32. [CrossRef]
18. Vishnevskij, A.A.; Kazbanov, V.V.; Batalov, M.S. Prospects for the use of titanium implants with specified osteogenic properties. *Russ. J. Spine Surg.* **2016**, *13*, 50–58.

19. Lam, T.-N.; Trinh, M.-G.; Huang, C.-C.; Kung, P.-C.; Huang, W.-C.; Chang, W.; Amalia, L.; Chin, H.-H.; Tsou, N.-T.; Shih, S.-J.; et al. Investigation of bone growth in additive-manufactured pedicle screw implant by using Ti-6Al-4V and bioactive glass powder composite. *Int. J. Mol. Sci.* **2020**, *21*, 7438. [CrossRef] [PubMed]
20. Galetsky, I.A.; Mishigdorzhiyn, U.L.; Semenov, A.P.; Yuzhakov, I.A.; Ulakhanov, N.S.; Burkov, A.G.; Semenov, E.D.; Tihonov, A.G.; Shustov, A.I. Methods for forming the performance properties of products from titanium alloys produced using additive technologies AT atmospheric pressure in the tip plane system. In Proceedings of the VIII International Scientific Conference Problems of Mechanics of Modern Machines, Ulan-Ude, Russia, 4–9 July 2022.
21. Grishunin, V.A.; Gromov, V.E.; Ivanov, Y.F.; Yuryev, A.B.; Vorobyev, S.V. Increase of the fatigue life of the rail steel by electron beam treatment. *Ferr. Metall.* **2013**, *56*, 51–54. (In Russian) [CrossRef]
22. Komissarova, I.A.; Konovalov, S.V.; Kosinov, D.A.; Feoktistov, A.V.; Ivanov, Y.F.; Gromov, V.E. Formation and evolution of the structure and phase composition of titanium VT 1-0 during electron beam processing, current pulse action, and multi-cycle fatigue. In *Anthology of Strength and Ductility of Metals and Alloys Under External Energy Influences*; Gromov, V.E., Ed.; Publishing SibSIU: Novokuzneck, Russia, 2018; pp. 62–81.
23. Shpanov, D.A.; Moskvin, P.V.; Petrikova, E.A.; Ivanov, Y.F.; Vorobyov, M.S. Control of the electron beam current during the pulse for alloying the surface of stainless steel with titanium and aluminum. *Mater. Technol. Des.* **2024**, *6*, 129–141. [CrossRef]
24. Koval, N.N.; Teresov, A.D.; Shtejnle, A.V. Polishing the surface of the spokes of the transosseous osteosynthesis apparatus using a pulsed electron beam of submillisecond duration followed by their sharpening. *Bull. Tomsk. Polytech. Univ.* **2011**, *318*, 116–120.
25. Bagautdinov, R.R.; Makarov, I.V. General recommendations on the choice of cutting modes for processing titanium alloys. *A Young Sci.* **2021**, *382*, 15–17.
26. Wennerberg, A.; Albrektsson, T. Effects of titanium surface topography on bone integration: A systematic review. *Clin. Oral Implant. Res.* **2009**, *20*, 172–184. [CrossRef]
27. Savilov, A.V.; Svinin, V.M.; Timofeev, S.A. Studies on Titanium Alloy Turning Rate Improvement. In Proceedings of the 5th International Conference on Industrial Engineering (ICIE 2019), Sochi, Russia, 25–29 March 2019.
28. Koval, N.N.; Devyatkov, V.N.; Vorobyev, M.S. Electron Sources with Plasma Grid Emitters: Progress and Prospects. *Russ. Phys. J.* **2021**, *63*, 1651–1660. [CrossRef]
29. Koval, N.N.; Devyatkov, V.N.; Vorobyov, M.S. Grid plasma cathodes: History, status, prospects. *Bull. Russ. Acad. Sci. Phys.* **2023**, *87*, S288–S293. [CrossRef]
30. Devyatkov, V.N.; Koval, N.N.; Schanin, P.M.; Grigoryev, V.P.; Koval, T.V. Generation and propagation of high-current low-energy electron beams. *Laser Part. Beams* **2003**, *21*, 243. [CrossRef]
31. Shin, V.I.; Vorobyov, M.S.; Moskvin, P.V.; Devyatkov, V.N.; Koval, N.N.; Mokeev, M.A. Generation of an electron beam in a source with a plasma emitter in the combined current control mode. *Bull. Russ. Acad. Sci. Phys.* **2023**, *87*, S324–S327. [CrossRef]
32. Shin, V.I.; Moskvin, P.V.; Vorobyev, M.S.; Devyatkov, V.N.; Doroshkevich, S.Y.; Koval, N.N. Increasing the electrical strength of the accelerating gap in an electron source with a plasma cathode. *Instrum. Exp. Tech.* **2021**, *64*, 234–240. [CrossRef]
33. Shin, V.I.; Vorobyov, M.S.; Moskvin, P.V.; Devyatkov, V.N.; Yakovlev, V.V.; Koval, N.N.; Torba, M.S.; Kartavtsov, R.A.; Vorobyov, S.A. Latitude and amplitude modulation of the beam current for controlling its power during a submillisecond pulse. *Russ. Phys. J.* **2023**, *65*, 1979–1988. [CrossRef]
34. Vorobyov, M.S.; Moskvin, P.V.; Shin, V.I.; Koval, N.N.; Ashurova, K.T.; Doroshkevich, S.Y.; Devyatkov, V.N.; Torba, M.S.; Levanisov, V.A. Dynamic Power Control of a Submillisecond Pulsed Megawatt Electron Beam in a Source with a Plasma Cathode. *Tech. Phys. Lett.* **2021**, *47*, 528–531. [CrossRef]
35. Vorobyov, M.S.; Koval, T.V.; Shin, V.I.; Moskvin, P.V.; Tran, M.K.A.; Koval, N.N.; Ashurova, K.; Doroshkevich, S.Y.; Torba, M.S. Controlling the Specimen Surface Temperature during Irradiation with a Submillisecond Electron Beam Produced by a Plasma-Cathode Electron Source. *IEEE Trans. Plasma Sci.* **2021**, *49*, 2550–2553. [CrossRef]
36. Devyatkov, V.N.; Mokeev, M.A.; Vorobyov, M.S.; Koval, N.N.; Moskvin, P.V.; Kartavtsov, R.A.; Doroshkevich, S.Y.; Torba, M.S. Electron source with a multi-arc plasma cathode for generating a modulated beam of submillisecond duration. *Tech. Phys. Lett.* **2024**, *50*, 20–23.
37. Vorobyov, M.S.; Petrikova, E.A.; Shin, V.I.; Moskvin, P.V.; Ivanov, Y.F.; Koval, N.N.; Koval, T.V.; Prokopenko, N.A.; Kartavtsov, R.A.; Shpanov, D.A. Steel surface doped with Nb via modulated electron-beam irradiation: Structure and properties. *Coatings* **2023**, *13*, 1131. [CrossRef]
38. Vorobyov, M.S.; Ashurova, K.T.; Ivanov, Y.F.; Moskvin, P.V.; Petrikova, E.A.; Petyukevich, M.S.; Rygina, M.E.; Shin, V.I.; Doroshkevich, S.Y. Treatment of silumin surface by a modulated submillisecond electron beam. *High Temp. Mater. Process.* **2022**, *26*, 1–10. [CrossRef]
39. Gromov, V.E.; Ivanov, Y.F.; Vorobiev, S.V.; Konovalov, S.V. *Fatigue of Steels Modified by High Intensity Electron Beams*; Cambridge International Science Publishing Ltd.: Cambridge, UK, 2015; p. 272.
40. Valiev, R.Z.; Islamgaliev, R.K.; Alexandrov, I.V. Bulk nanostructured materials from severe plastic deformation. *Prog. Mater. Sci.* **2000**, *45*, 103–189. [CrossRef]

41. Schwartz, Z.; Raz, P.; Zhao, G.; Barak, Y. Effect of Micrometer-Scale Roughness of the Surface of Ti6Al4V Pedicle Screws in Vitro and in Vivo. *JBJS* **2008**, *90*, 2485–2498. [CrossRef] [PubMed]
42. Akhmadeev, Y.H.; Denisov, V.V.; Ivanov, Y.F. *Electron–Ion–Plasma Modification of the Surface of Nonferrous Metals and Alloys*; Koval, N.N., Ivanov, Y.F., Eds.; NTL Publishing House: Tomsk, Russia, 2016; p. 312. (In Russian)
43. Jo, W.L.; Lim, Y.W.; Kwon, S.Y.; Bahk, J.-H.; Kim, J.; Shin, T.; Kim, Y.H. Non-thermal atmospheric pressure plasma treatment increases hydrophilicity and promotes cell growth on titanium alloys in vitro. *Sci. Rep.* **2023**, *13*, 14792. [CrossRef]
44. Wang, M.; Peng, Z.; Li, C.; Zhang, J.; Wu, J.; Wang, F.; Li, Y.; Lan, H. Multi-Scale Structure and Directional Hydrophobicity ofTitanium Alloy Surface UsingElectrical Discharge. *Micromachines* **2022**, *13*, 937. [CrossRef]
45. Toh, W.Q.; Wang, P.; Tan, X.; Nai, M.L.S.; Liu, E.; Tor, S.B. Microstructure and Wear Properties of Electron Beam Melted Ti-6Al-4V Parts: A Comparison Study against As-Cast Form. *Metals* **2016**, *6*, 284. [CrossRef]
46. Köse, C.; Karaca, E. Robotic Nd:YAG Fiber Laser Welding of Ti-6Al-4V Alloy. *Metals* **2017**, *7*, 221. [CrossRef]
47. Martinez, M.A.F.; Balderrama, Í.; Karam, P.S.B.H.; Oliveira, R.C.; Oliveira, F.A.; Grandini, C.R.; Vicente, F.B.; Stavropoulos, A.; Zangrando, M.S.R.; Sant'Ana, A.C.P. Surface roughness of titanium disks influences the adhesion, proliferation and differentiation of osteogenic properties derived from human. *Int. J. Implant. Dent.* **2020**, *6*, 46. [CrossRef]
48. Jabbari, Y.A.; Mueller, W.D.; Al-Rasheed, A.; Zinelis, S. The Effects of Surface Roughening Techniques on Surface and Electrochemical Properties of Ti Implants. In *Dental Implantology and Biomaterial*; Almasri, M.A.J.A., Ed.; InTech: London, UK, 2016. [CrossRef]
49. Zinelis, S. *Surface and Electrochemical Characterization of Contemporary Ti Implants with Different Surface Modifications*; National and Kapodistrian University of Athens: Athens, Greece, 2016.
50. Albrektsson, T.; Wennerberg, A. Oral implant surfaces: Part 2—Review focusing on clinical knowledge of different surfaces. *Int. J. Prosthodont.* **2004**, *17*, 544–564. [PubMed]
51. Sun, Y.; Bailey, R.; Zhang, J.; Lian, Y.; Ji, X. Effect of thermal oxidation on the dry sliding friction and wear behaviour of CP-Ti on CP-Ti tribopairs. *Surf. Sci. Technol.* **2023**, *1*, 15. [CrossRef]
52. Braic, M.; Braic, V.; Vladescu, A.; Zoita, C.N.; Balaceanu, M. Solid solution or amorphous phase formation in TiZr-based ternary to quinternarymulti-principal-element films. *Prog. Nat. Sci.* **2014**, *24*, 305–312. [CrossRef]
53. Shen, W.-J.; Tsai, M.-H.; Yeh, J.-W. Machining performance of sputter-deposited (Al0.34Cr0.22Nb0.11Si0.11Ti0.22)50 N50 high-entropy nitride coatings. *Coatings* **2015**, *5*, 312–325. [CrossRef]
54. An, Z.; Jia, H.; Wu, Y.; Rack, P.D.; Patchen, A.D.; Liu, Y.; Ren, Y.; Li, N.; Liaw, P.K. Solid-solution CrCoCuFeNi high-entropy alloy thin films synthesized by sputter deposition. *Mater. Res. Lett.* **2015**, *3*, 203–209. [CrossRef]
55. Ji, X.; Duan, H.; Zhang, H.; Ma, J. Slurry erosion resistance of laser clad NiCoCrFeAl3 high-entropy alloy coatings. *Tribol. Trans.* **2015**, *58*, 1119–1123. [CrossRef]
56. Zhang, H.; Wu, W.; He, Y.; Li, M.; Guo, S. Formation of core–shell structure in high entropy alloy coating by laser cladding. *Appl. Surf. Sci.* **2016**, *363*, 543–547. [CrossRef]
57. Yue, T.; Xie, H.; Lin, X.; Yang, H.; Meng, G. Microstructure of laser remelted AlCoCrCuFeNi high entropy alloy coatings produced by plasma spraying. *Entropy* **2013**, *15*, 2833–2845. [CrossRef]
58. Yao, C.-Z.; Zhang, P.; Liu, M.; Li, G.R.; Ye, J.Q.; Liu, P.; Tong, Y.X. Electrochemical preparation and magnetic study of Bi–Fe–Co–Ni–Mn high entropy alloy. *Electrochim. Acta* **2008**, *53*, 8359–8365. [CrossRef]
59. Liu, D.; Cheng, J.B.; Ling, H. Electrochemical behaviours of (NiCoFeCrCu)95 B5 high entropy alloy coatings. *Mater. Sci. Technol.* **2015**, *31*, 1159–1164. [CrossRef]
60. Katakam, S.; Joshi, S.S.; Mridha, S.; Dahotre, N.B. Laser assisted high entropy alloy coating on aluminum: Microstructural evolution. *J. Appl. Phys.* **2014**, *116*, 104–106. [CrossRef]

Disclaimer/Publisher's Note: The statements, opinions and data contained in all publications are solely those of the individual author(s) and contributor(s) and not of MDPI and/or the editor(s). MDPI and/or the editor(s) disclaim responsibility for any injury to people or property resulting from any ideas, methods, instructions or products referred to in the content.